Journal of Catalysis **185,** 12–22 (1999)
Article ID jcat.1999.2498, available online at http://www.idealibrary.com on IDEAL®

Methane Dissociation and Syngas Formation on Ru, Os, Rh, Ir, Pd, Pt, Cu, Ag, and Au: A Theoretical Study

Chak-Tong Au,* Ching-Fai Ng,* and Meng-Sheng Liao†,[1]

*Department of Chemistry, Hong Kong Baptist University, Kowloon, Hong Kong; and †Department of Chemistry, Xiamen University, Xiamen 361005, P. R. China

Received March 1, 1999; accepted March 29, 1999

A theoretical study of methane dissociation and syngas formation on a number of transition metals M (M = Ru, Os, Rh, Ir, Pd, Pt, Cu, Ag, Au) is presented. The metal surface is simulated by a M_{10} cluster model. Reaction energies for the steps involved are determined. The activation energies have been estimated using the analytic BOC-MP formula. The dissociation energy is shown to be an important factor determining the catalytic activity of the metal. The order of the calculated total dissociation energies ($CH_{4,s} \rightarrow C_s + 4H_s$) is consistent with the order of methane conversions over the metals. In the presence of adsorbed oxygen, oxygen at metal on-top sites promotes methane dehydrogenation; oxygen at hollow sites promotes methane dehydrogenation on Pt, Cu, Ag, and Au, but shows no such effect on the other transition metals. The difference in the H_2 selectivities can be associated with the difference in the stabilities of OH on the metals. For CH_x couplings, the trend in the calculated combination energies is in agreement with experimental observation.

INTRODUCTION

Methane conversion to higher hydrocarbons is of worldwide interest. Several processes have been proposed. A possible route is the oxidative coupling of methane (OCM) reaction to C_2 hydrocarbons (1). However, the OCM to C_2s seems to be too difficult to reach an economical scale. Current practice of converting CH_4 into higher hydrocarbons proceeds by the indirect route in which methane is first converted to syngas. Syngas production is currently achieved commercially by steam reforming according to the water gas shift reaction:

$$CH_4 + H_2O \rightarrow CO + 3H_2. \quad [1]$$

This process suffers from disadvantages of high energy requirement, high H_2/CO ratio (>4, which is not suitable for methanol and Fischer–Tropsch synthesis), and poor selectivity for CO. In recent years, there has been considerable interest in the catalysis of selective partial oxidation of methane to syngas (here denoted as OMS):

$$CH_4 + \tfrac{1}{2}O_2 \rightarrow CO + 2H_2. \quad [2]$$

The OMS reaction is mildly exothermic, more selective, and produces the desired $H_2/CO = 2/1$ ratio. Recently, a series of supported transition metals (Ru, Os, Rh, Ir, Ni, Pd, ...) were found to be active in OMS reaction (2–14).

The mechanism for the catalytic OMS has been studied by a number of authors. Since the early work of Prettre *et al.* (15), it has been accepted that the reaction process involves first the oxidation of CH_4 primarily to H_2O and CO_2 followed by the reforming of CH_4 with H_2O and/or CO_2 formed in the first stage. Various data have been presented in support of this opinion (2–4). The other mechanism is direct oxidation via methane pyrolysis as proposed by Schmidt *et al.* (5, 6), based on experiments over monolith-supported Rh and Pt catalysts at short contact time. According to the latter authors, the dissociation of methane is an initial step; H_2 and CO are formed via surface species (CH_x, H) originated from methane dissociation. The latter mechanism has been supported by a series of recent pulse studies (8–14). It was concluded that CH_4 conversion depends on its dissociation steps (13).

The catalysis of the OMS reaction is rather complex and the experimental conditions adopted may influence the reaction steps strongly. From the various studies (2–15), one may agree that the contact time between reactant and catalyst is a critical factor that can affect the reaction scheme, as claimed by Schmidt *et al.* (6). It is, therefore, expected that the shortening of residence times can induce direct catalytic OMS.

On the basis of the methane pyrolysis mechanism, there are the following possible reaction steps (g, gas; s, surface):

$$O_{2,g} + \text{site} \rightarrow 2O_s \quad [3]$$

$$CH_{4,g} + \text{site} \rightarrow CH_{x,s} + (4-x)H_s \rightarrow C_s + 4H_s \quad [4]$$

[1] Present address: Department of Chemistry, University of Puerto Rico, P.O. Box 23346, San Juan, PR 00931.

0021-9517/99 $30.00

$$C_s + O_s \rightarrow CO_s \rightarrow CO_g \quad [5]$$

$$H_s + H_s \rightarrow H_{2,s} \rightarrow H_{2,g}. \quad [6]$$

According to the results of pulse studies (13, 14), the unreduced catalysts which contain metal oxides give much lower CH_4 conversion and CO selectivity than the freshly reduced catalysts. On the other hand, support materials has relatively little influence on catalytic activities (5c). It was therefore concluded that reduced metals are the main active site for syngas formation.

In this paper, we want to perform a theoretical study for the dissociation of methane and the formation of syngas on a number of transition metals M ($M =$ Ru, Os, Rh, Ir, Pd, Pt, Cu, Ag, and Au), thereby extending the previous work (16). Here we have not included Ni in the study because we had the SCF convergence problem with a large Ni_n cluster model. Experimentally (6), the Ni and Rh catalysts showed similar conversions and selectivities, but Ni deactivated. Both Ni and Rh exhibited higher activity in the OMS reaction than other metal catalysts. Coinage metals (Cu, Ag, Au) are known to be far less active (12). A theoretical comparative study of these systems would be of interest to evaluate the variation in catalytic abilities among these metals. Because it is difficult to locate the transition states for the reactions on the metal surfaces, we focus mainly on an evaluation of the surface dissociation energies which should be an important determining factor in the OMS process. Shustorovich (17, 18) has developed the so-called bond-order conversion Morse-potential (BOC-MP) method to treat the dissociations of adsorbates on metal surfaces. The analytic BOC-MP formula relates the activation energy to the adsorption energies of an adsorbate and its dissociative fragments. The BOC-MP method is a simple, but a reasonable way of getting estimates of energy barriers quickly (18). Very recently, Shustorovich and Sellers (19) have made a considerable revision to the BOC-MP approach. They also give a change of the method's name, namely the unity bond index–quadratic exponential potential (UBI-QEP) method. However, the analytic expression for estimating activation barriers remains unchanged.

COMPUTATIONAL METHOD AND METAL SURFACE MODELING

The quantum chemical calculations reported in this paper were carried out using the Amsterdam density-functional (ADF) program package developed by Baerends *et al.* (20). The main features of the ADF method are the use of the LCSTO expansion technique and frozen-core approximation. The bond energy is evaluated by the so-called "transition state method" (21), which represents an important advantage of the ADF program package. Relativistic corrections are calculated by the quasirelativistic method (22). Many useful exchange-correlation potential functionals are included. They are Slater's X_α exchange, Vosko–Wilk–Nusair correction (VWN) (23), Becke's gradient correction for exchange (B) (24), the Perdew–Wang gradient correction for exchange (PWx) (25), Stoll's self-interaction correction for correlation (S) (26), and Perdew's gradient correction for correlation (P) (27). These can be combined to give various functionals.

In this work, the VWN–B–P functional, as in our previous calculations (16), was used. For C and O, the 1s shell was frozen. For the metal atoms, the electrons up to and including $(n-1)p$ shells were kept frozen. Triple-zeta STO basis sets were employed for the metal $(n-1)d$–ns, C/O 2s–2p, and H 1s valence shells. Single-zeta STOs are used for core orthogonalization. Polarization functions have been added to the valence bases: one p-type polarization function for the metals, one d-type polarization function for C and O, and one p-type polarization function for H.

We chose metal $M(111)$ as the surface for adsorption, $M(111)$ is simulated by a two-layer-thick $M_{10}(n_1, 10-n_1)$ cluster which contains n_1 metal atoms in the first layer and $10-n_1$ in the second. Here n_1 is 7 or 3, depending on the model (on-top site model or threefold hollow site model) used. In order to examine the influence of cluster size on the calculated results, a larger M_{13} cluster, where $M(7, 6)$ represents an on-top site model and $M(6, 7)$ a hollow site model, was also tested for $M =$ Pd and Cu. So far, one has still little idea about how many atoms should be used to describe a metal surface. An increase of cluster size will greatly increase the computational time. In some cases, one found a large oscillation of adsorption energies with cluster size (28, 29). Siegbahn and coworkers (29) have suggested so-called "bond-prepared states" for calculating chemisorption energies of σ-bonded adsorbates. We do not choose to apply this method at present because we have not performed a systematic test of this rule within the ADF framework. On the other hand, the rule is applicable only to adsorbates with a single radical electron, like H and CH_3. For adsorbates with double radical electrons, like O or CO, the rule is not so satisfactory (29).

The geometries used in the calculation are shown in Fig. 1. The parts above the metal surfaces were fully optimized under the constraint of the symmetries given in the pictures. The O–H bond was found to be perpendicular to the surfaces. The cluster geometries were held fixed in the calculations, and the M–M distances were based on the bulk crystal data.

RESULTS AND DISCUSSION

Adsorption Energies of Intermediate Fragments (CH_x, H, O)

Methane decomposition on "reduced transition metals" results in the formation of CH_x ($x = 3, 2, 1, 0$) and H

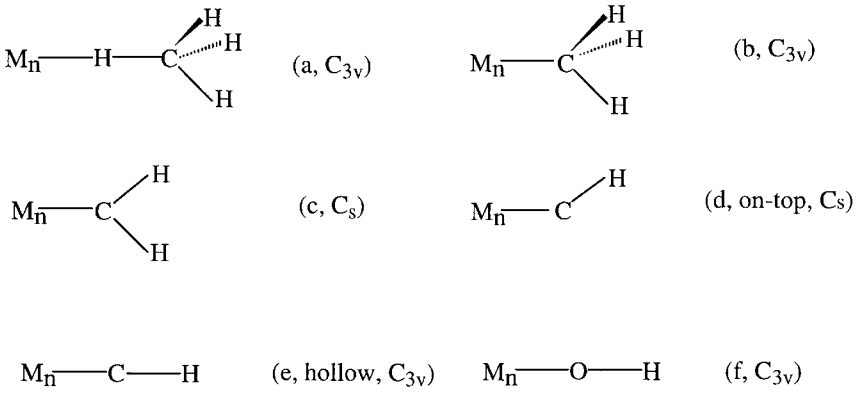

FIG. 1. Models for the CH_x ($x = 4, \ldots, 1$) and OH species adsorbed on the metal cluster M_n.

adspecies, so the adsorption energies of the various species bear an essential implication in methane dissociation and syngas formation. The results are collected in Table 1, together with available experimental data. The preferred sites for the adspecies have been identified. At present, only two sites, viz. on-top and threefold hollow, are considered. Table 2 gives the calculated heights of the species above the metal surfaces. We have not listed the other calculated geometry parameters. It was found that the C–H and O–H bond lengths change only slightly from the free species to the adsorbed ones and the umbrella angles in adsorbed CH_4 and CH_3 are nearly equal to the tetrahedral one. Table 3 shows the Mulliken charge distributions on the whole adsorbed species.

For the adsorption of CH_4 on the metal surfaces, the adsorption energies involved are small, with magnitudes less than 0.2 eV. This is to be expected as CH_4 is a saturated molecule. The on-top site is more favorable for the adsorption of CH_4. The M–H distances are generally large, especially the Ag–H one. The Ir–H and Pt–H distances are relatively small. Due to the close approach, there is a small charge transfer from Ir_{10} or Pt_{10} to CH_4. On the other metal clusters, charge transfer occurs from the adsorbed species to M_{10}.

CH_3 can adsorb rather strongly on the metal surfaces. The calculated adsorption energies are 1.5–2.0 eV on the transition metals (Ru–Pt) and 0.5–1.2 eV on the coinage metals (Cu–Au). The preferred bonding sites vary among the metals. On Ru, Rh, and Cu, the hollow site is preferred, while the on-top site is preferred on the other metals for adsorbed CH_3. It is found that energy differences (Δ) between the sites are small on Rh ($\Delta = 0.14$ eV), Os ($\Delta = 0.06$ eV), and Ag ($\Delta = 0.06$ eV).

For the adsorption of CH_2, CH, and C, the hollow site is clearly preferred. The difference in the adsorption energies between the on-top and the hollow sites is large. Therefore, unsaturated C in these species has a strong tendency to recover its missing bonds, in agreement with the extended Hückel band calculations by Hoffmann *et al.* (30). The adsorption energy of CH_x on a given transition metal increases from $x = 3$ to $x = 0$. The increase is large from CH_2 to CH, but is much less from CH to C. On the coinage metals, C has the adsorption energy which is smaller than that of CH. To facilitate comparison of the calculated adsorption energies (E) among the CH_x species and among the metals (M), plots of E versus x and M are shown in Fig. 2.

H is found to prefer the on-top site on Os and Ir. On the other metals, the hollow site is preferred. Experimental data of the adsorption energy of H are known for many metals. All the calculated values are close to the experimental results, with typical error not exceeding 0.3 eV. For $M =$ Ag and Au, experimental studies suggested that the values are less than 2.5 eV. The calculated results are 1.6–1.8 eV, in agreement with the experimental predictions.

Similar to C, O strongly prefers the hollow site of the metal surfaces. For $M =$ Pd, Pt, and Cu–Au, the calculated

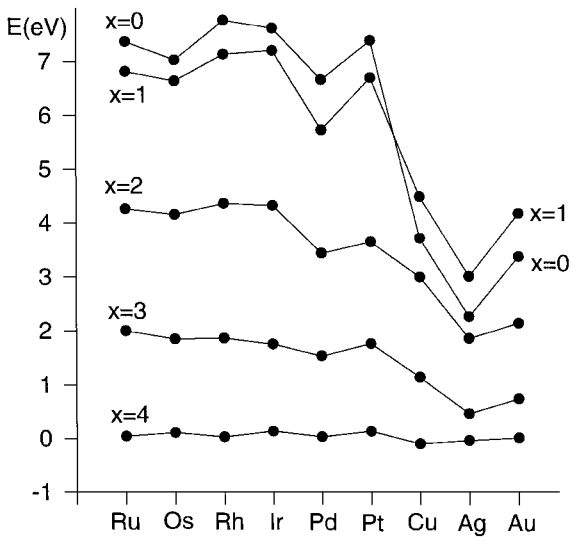

FIG. 2. Schematic illustration of calculated adsorption energies for the CH_x species on the metal $M(111)$ surfaces.

TABLE 1

Calculated Adsorption Energies[a] E (eV) for Various Species Adsorbed on the M_{10} (n, 10 − n) Cluster Model of M(111)

(a) on Ru, Rh, and Pd

	Ru(7, 3) (top)	Ru(3, 7) (hol)	Exptl	Rh(7, 3) (top)	Rh(3, 7) (hol)	Exptl	Pd(7, 3) (top)	Pd(3, 7) (hol)	Exptl
CH_4	0.04	−0.24		0.03	−0.06		0.04	0.02	
							0.02[b]	0.01[b]	
CH_3	1.55	2.00		1.73	1.87		1.54	1.12	
							1.66	1.07	
CH_2	3.11	4.26		3.09	4.37		2.14	3.45	
							2.61	3.28	
CH	4.21	6.81		3.92	7.14		3.60	5.74	
							3.26	6.19	
C	5.25	7.37		5.09	7.77		4.43	6.67	
							4.19	6.82	
H	2.53	2.82	2.91	2.57	2.89	2.65	2.35	2.61	2.69
							2.46	2.70	
O	4.42	6.24	4.34	3.64	6.67	4.42	3.15	4.09	3.77
							2.71	4.23	
H → O[c]	2.78	2.74		2.94	2.57		3.32	2.51	
							3.45	2.88	
OH	2.24	4.03		1.63	3.68		1.52	1.65	
							1.15	2.16	

(b) on Os, Ir, and Pt

	Os(7, 3) (top)	Os(3, 7) (hol)		Ir(7, 3) (top)	Ir(3, 7) (hol)	Exptl	Pt(7, 3) (top)	Pt(3, 7) (hol)	Exptl
CH_4	0.11	−0.24		0.14	−0.12		0.14	0.05	
CH_3	1.85	1.79		1.76	1.50		1.77	1.23	
CH_2	3.19	4.16		3.18	4.33		3.03	3.66	
CH	4.01	6.64		3.56	7.21		3.80	6.71	
C	4.51	7.03		4.71	7.63		4.61	7.40	
H	2.67	2.47		2.71	2.51	2.52	2.44	2.59	2.65
O	4.49	6.15		3.13	5.62	4.03	2.71	4.24	3.69
H → O	2.70	2.44		3.17	2.58		3.34	2.91	
OH	2.23	3.64		1.34	3.25		1.09	2.20	2.60[d]
								2.56[e]	

(c) On Cu, Ag, and Au

	Cu(7, 3) (top)	Cu(3, 7) (hol)	Exptl	Ag(7, 3) (top)	Ag(3, 7) (hol)	Exptl	Au(7, 3) (top)	Au(3, 7) (hol)	Exptl
CH_4	−0.09	−0.13		−0.03	−0.10		0.02	−0.03	
	−0.10	−0.11							
CH_3	0.65	1.15		0.47	0.41		0.75	0.38	
	0.81	1.28							
CH_2	1.23	3.01		0.78	1.87		0.93	2.15	
	1.57	2.75							
CH	1.70	4.50		1.06	3.02		1.27	4.19	
	2.17	4.51							
C	1.45	3.73		0.63	2.27		0.99	3.39	
	2.17	3.89							
H	1.32	2.12	2.43	1.19	1.63	<2.47	1.45	1.81	≤2.52
	1.58	2.28							
O	2.28	5.07	4.47	1.66	3.60	3.47	0.89	3.12	≤3.25
	2.58	4.67							
H → O	4.49	2.67		4.75	3.51		4.68	3.18	
	4.21	3.12							
OH	1.82	2.79		1.46	2.16		0.62	1.35	
	1.84	2.94							

[a] Experimental data on M(111) are those cited in Ref. (18).
[b] Values in the "second" row are results calculated on the M_{13} cluster; the same is true for the other species.
[c] Represents adsorption of H on surface O.
[d] From Ref. (36).
[e] Calculated using the UBI-QEP method (19).

TABLE 2

Calculated Heights (in Å) above the Metal Surface

	Ru_{10}	Os_{10}	Rh_{10}	Ir_{10}	Pd_{10}	Pt_{10}	Cu_{10}	Ag_{10}	Au_{10}
CH_4									
t	2.20	2.19	2.19	2.02	2.10	2.05	2.29	2.70	2.30
h	2.04	2.16	2.32	2.15	2.15	2.10	2.29	2.30	2.30
CH_3									
t	2.04	2.17	2.03	2.05	2.04	2.08	2.07	2.25	2.16
h	1.61	1.95	1.70	2.03	1.73	1.73	1.65	2.04	2.03
CH_2									
t	1.95	1.96	1.90	1.89	1.88	1.90	1.93	2.14	2.05
h	1.50	1.62	1.41	1.53	1.35	1.36	1.40	1.55	1.49
CH									
t	1.73	1.85	1.75	1.76	1.81	1.79	1.88	2.10	2.02
h	1.24	1.42	1.15	1.16	1.09	1.18	1.19	1.27	1.16
C									
t	1.67	1.80	1.66	1.69	1.74	1.77	1.82	2.01	1.94
h	1.22	1.28	1.11	1.19	1.03	1.05	1.24	1.38	0.98
H									
t	1.64	1.67	1.58	1.64	1.53	1.56	1.54	1.70	1.62
h	1.04	1.25	0.95	0.99	0.78	0.80	0.94	0.94	0.82
O									
t	1.71	1.81	1.72	1.75	1.87	1.87	1.80	2.07	2.05
h	1.26	1.41	1.16	1.26	1.20	1.21	1.22	1.40	1.40
HO									
t	1.90	1.98	1.92	1.91	2.07	2.08	1.94	2.19	2.28
h	1.56	1.78	1.62	1.70	1.62	1.65	1.46	1.75	1.73

Note. t, top; h, hollow.

and experimental adsorption energies are comparable. For $M =$ Ru, Rh, and Ir, however, the calculated Es are 1.5–2.2 eV too large. The large adsorption energies of O indicate that O can be trapped strongly on the metal surface. This agrees with various experimental evidences. The net charge of the adsorbed O (O_s) is higher at the hollow site than at the on-top site. Torras *et al.* (31) have performed an investigation for bondings of O on Cu and Ag. A $M_5(4, 1)$ cluster was used to simulate the $M(100)$ surface. For O at the fourfold site, they get net Mulliken charges on O which are very similar for the two metals (~ -1.5 e). Our calculated charges for O on the two metals (~ -0.8 e) are in qualitative agreement with those estimated by Torras *et al.* In fact the data in Table 3 may only provide a rough qualitative idea of the charge distribution. We must caution that Mulliken population analysis is not free of artifacts (32); it may give misleading information about atomic charges (33, 34). The natural population analysis (NPA) (35) is an alternative to Mulliken population analysis; it was shown to exhibit improved numerical stability. The NPA method has been attached to variety of *ab initio* program package (Gaussian, Gamess, etc.). Nevertheless, Mulliken population analysis has widely been used until now.

The H species produced in methane dissociation may react with O_s to form HO_s. Hence we have calculated the adsorption energies of H on O_s, $E(H \rightarrow O)$. The E values depend strongly on the position at which the O is located. Compared to the bare metal surfaces, the presence of O^{top} increases the adsorption energy of H, but the magnitude of the increase in E_{ads} differs on different metals. The presence of O^{hol} increases the adsorption energies of H on Pt and Cu–Au, but displays an opposite effect on the other metals. On the other hand, $E(H \rightarrow O^{top})$ is larger than $E(H \rightarrow O^{hol})$. After H adsorption, the M–O^{top} distance is expanded by 0.15–0.2 Å. The expansion of M–O^{hol} is more pronounced, by 0.3–0.4 Å. We have also listed the calculated adsorption energies of OH. Experimental as well as UBI-QEP data of E_{ads} exist for OH on Pt(111) (36, 19). Our calculated value (2.2 eV) can be found to be in reasonable agreement with these data (2.6 eV).

We see that the adsorption energies calculated on the M_{13} cluster are quite close to those on the M_{10} cluster. Especially, the calculated dissociation energies as well as the activation barriers on M_{10} and M_{13} do not deviate significantly (see Tables 4 and 5). Because the difference in size between M_{10} and M_{13} is not very large, we may not arrive at a conclusion that the cluster size effect on the calculated adsorption energies is small. As pointed out above, one has to be aware of the limitations in the cluster approximation. However, the main purpose of this paper is to compare the various metals at the same level of theoretical treatment,

TABLE 3

Mulliken Charge Distributions (in e) on the Whole Adsorbed Species

	Ru_{10}	Os_{10}	Rh_{10}	Ir_{10}	Pd_{10}	Pt_{10}	Cu_{10}	Ag_{10}	Au_{10}
CH_4									
t	0.12	0.01	0.10	−0.09	0.15	−0.08	0.18	0.10	0.09
h	0.20	−0.01	0.12	−0.01	0.30	−0.02	0.14	0.08	−0.04
CH_3									
t	−0.19	−0.17	−0.23	−0.20	−0.32	−0.40	0.00	−0.17	−0.27
h	−0.75	−0.51	−0.47	−0.34	−0.64	−0.78	−0.02	−0.05	−0.34
CH_2									
t	−0.32	−0.43	−0.35	−0.42	−0.41	−0.49	−0.04	−0.28	−0.45
h	−0.88	−1.13	−0.86	−1.12	−1.02	−1.32	−0.46	−0.67	−1.41
CH									
t	−0.41	−0.48	−0.39	−0.56	−0.46	−1.04	−0.11	−0.32	−0.44
h	−1.18	−1.49	−1.11	−1.78	−1.27	−1.72	−0.79	−1.19	−2.10
C									
t	−0.32	−0.47	−0.32	−0.46	−0.33	−0.55	−0.10	−0.35	−0.43
h	−0.80	−1.00	−0.79	−1.06	−0.89	−1.30	−0.51	−0.65	−1.88
H									
t	−0.22	−0.24	−0.31	−0.19	−0.40	−0.24	−0.14	−0.39	−0.50
h	−0.42	−0.48	−0.38	−0.64	−0.82	−0.89	−0.07	−0.33	−0.98
O									
t	−0.51	−0.50	−0.54	−0.51	−0.54	−0.54	−0.65	−0.69	−0.58
h	−0.92	−0.92	−0.90	−0.94	−0.86	−0.98	−0.82	−0.83	−0.86
HO									
t	−0.39	−0.39	−0.44	−0.44	−0.44	−0.44	−0.45	−0.56	−0.46
h	−0.56	−0.48	−0.46	−0.44	−0.59	−0.48	−0.43	−0.51	−0.49

Note. t, top; h, hollow.

TABLE 4

Calculated Dissociation Energies $D_{e,s}$ (eV) (Scheme 7)

	Ru_{10}	Os_{10}	Rh_{10}	Ir_{10}	Pd_{10}	Pt_{10}	Cu_{10}	Ag_{10}	Au_{10}
$CH_{4,s} \rightarrow CH_{3,s} + H_s$	0.06	0.44	0.12	0.50	0.71	0.63	1.60	2.76	2.31
					0.54[a]		1.30[a]		
$CH_{3,s} \rightarrow CH_{2,s} + H_s$	0.05	0.15	−0.26	−0.15	0.82	0.65	1.15	2.33	1.92
					0.81		1.38		
$CH_{2,s} \rightarrow CH_s + H_s$	−0.44	−0.22	−0.73	−0.66	−0.24	−0.71	1.32	2.15	1.08
					−0.68		0.89		
$CH_s \rightarrow C_s + H_s$	0.34	0.66	0.20	0.59	0.15	0.44	2.37	2.84	2.71
					0.39		2.06		
$CH_{4,s} \rightarrow C_s + 4H_s$	0.01	1.03	−0.67	0.28	1.44	1.01	6.44	10.08	8.02
					1.06		5.63		

Note. s, surface.

[a] Results calculated on the M_{13} clusters; the same is true for the other reactions.

and one may assume that the uncertainties due to cluster size will affect the results for these metals in similar fashion. On the other hand, the main results given in Tables 4 and 5 refer to energy differences which always involve adsorbed species and not to the absolute values of adsorption energies. Hermann *et al.* (28) also showed that the chemical bonding of adsorbate on the metal does not change much with cluster size. So, relative energies may be more reliable than absolute energies.

Methane Dissociation

The calculated adsorption energies given in Table 1 together with the calculated C–H bond strengths in gas-phase $CH_{x,g}$ can be used to determine $D_{e,s}$. The scheme is

$$\begin{array}{ccc} CH_{x,s} & \xrightarrow{D_{e,s}} & CH_{x-1,s} + H_s \\ \uparrow -E_1 & & \uparrow -E_2 \qquad \uparrow -E_H \\ CH_{x,g} & \xrightarrow[D_{e,g}]{} & CH_{x-1,g} + H_g \end{array} \qquad [7]$$

$$D_{e,s} = D_{e,g} + E_1 - E_2 - E_H, \qquad [8]$$

where E_1, E_2, and E_H are the adsorption energies of CH_x, CH_{x-1}, and H, respectively; the term $D_{e,g}$ represents the dissociation energy of CH_x in the gas phase.

In order to acquire some ideas about the barrier heights, the BOC-MP approach developed by Shustorovich (17, 18)

TABLE 5

Calculated Activation Energies E^* (eV) (Eq. [9])

	Ru_{10}	Os_{10}	Rh_{10}	Ir_{10}	Pd_{10}	Pt_{10}	Cu_{10}	Ag_{10}	Au_{10}
$CH_{4,s} \rightarrow CH_{3,s} + H_s$	0.62	0.77	0.63	0.79	0.84	0.84	1.12	1.54	1.42
					0.77[a]		1.01[a]		
						0.45[b]			
					0.70[c]	0.78[c]			
				1.10[d]		1.25[e]			
$CH_{3,s} \rightarrow CH_{2,s} + H_s$	0.88	0.89	0.74	0.76	1.14	1.09	1.20	1.60	1.45
					1.15		1.31		
					1.09[c]	1.13[c]			
$CH_{2,s} \rightarrow CH_s + H_s$	0.78	0.84	0.67	0.66	0.79	0.58	1.38	1.61	1.17
					0.60		1.20		
$CH_s \rightarrow C_s + H_s$	1.19	1.30	1.16	1.30	1.02	1.18	1.86	1.90	1.95
					1.16		1.75		

Note. s, surface.

[a] The values in the "second" row are the results calculated on the M_{13} clusters; the same is true for the other reactions.

[b] From ASED-MO calculations of Anderson and Maloney on a Pt_{10} cluster of Pt(111) (44).

[c] Calculated using the UBI-QEP method (19).

[d] Experimental value for Ir(110) (43).

[e] Experimental value from Ref. (42).

is employed here to evaluate the activation energies. This approach has proven to be efficient for treating energetics of molecular adsorbates on transition metals. The analytic BOC-MP formula relates the activation energy E^* to the adsorption energies of an adsorbate and its dissociative fragments on the surface. For the $CH_{x,s} \rightarrow CH_{x-1,s} + H_s$ reaction, the formula is given as

$$E^* = \frac{1}{2}\left(D_{e,g} + \frac{E_2 E_H}{E_2 + E_H} + E_1 - E_2 - E_H\right)$$
$$= \frac{1}{2}\left(\frac{E_2 E_H}{E_2 + E_H} + D_{e,s}\right). \quad [9]$$

Here the energy terms are shown in Scheme 7. According to Eq. [9], the BOC-MP formula also reveals a correlation between the activation energy and dissociation energy for the reaction. The calculated dissociation energies and activation energies are given in Tables 4 and 5, respectively.

Because the interactions of methane with metal surfaces underlie many important catalytic processes, they have been the subject of great interest and intense investigation. Much experimental as well as theoretical work has been devoted to dissociation of methane on Ni surfaces (see references cited in Refs. (37) and (38)). However, there are relatively few studies of the topics on other metals. On the other hand, the early studies were mainly concerned with the one-step dehydrogenation of methane to methyl. First we review some of the early studies of CH_4 dissociation on the metals considered here.

Stewart and Ehrlich (39) were among the first to perform surface science mechanistic studies of CH_4 dissociative chemisorption. For CH_4 on a highly perfect Rh surface, they estimate an apparent activation energy of 0.30 eV based on a molecular beam experiment. In the later work on CH_4/Rh, Brass and Ehrlich (40) measured an activation energy of 0.48 eV. Luntz and Harris (41) pointed out that the "activation" energies deduced in such experiments are only apparent and are not related to the barrier heights. An actual energy barrier may be considerably higher. Schoofs *et al.* (42) have studied the dissociative chemisorption of CH_4 on clean Pt(111) with a supersonic molecular beam. They estimate a barrier of 1.25 eV from a tunneling model. Hamza *et al.* (43) performed a molecular beam experiment for CH_4 on Ir(110), obtaining a barrier of 1.10 eV.

On the theoretical side, Anderson and Maloney (44), using semiempirical ASED-MO method and clusters, have studied the activation of CH_4 on Pt(111). They calculate an activation barrier of 0.45 eV for CH_4 on a Pt_{10} cluster of Pt(111). Blomberg *et al.* (45) carried out CCI + Q calculations of methane activation over single Rh and Pd atoms. The barriers for the CH_3–H insertion by the atoms are determined to be 0.41 and 1.09 eV, respectively. Swang *et al.* (46) reported relativistic effective core potential (RECP) calculations of methane activation over a single Os atom. They obtained a barrier of 1.17 eV. In addition, there have been UBI-QEP calculations of activation barriers for $CH_x \rightarrow CH_{x-1} + H$ on Pd and Pt ($x = 4, 3$) (19); the calculated values are shown in Table 5 for comparison. It was claimed (19) that the UBI-QEP method provides reaction activation barriers with a typical accuracy of 1–3 kcal/mol (i.e., 0.1–0.2 eV).

Let us look at our results for the first dehydrogenation step. On Pt_{10}, the barrier is estimated to be 0.84 eV. This value is much larger than the ASED-MO value, but quite comparable to the UBI-QEP value. The calculation predicts a notably lower barrier than the experiment. The same is true for Ir_{10}. However, the calculated trend for Ir versus Pt agrees with the experimental one. The estimated barrier on Rh_{10} is rather low. This is consistent with the experimental evidences. Both our and CCI + Q calculations indicate that the barrier heights follow the order Rh < Pd. Concerning the second dehydrogenation step ($CH_{3,s} \rightarrow CH_{2,s} + H_s$), our estimated values are also close to the UBI-QEP data.

The dehydrogenation of CH_x to CH_{x-1} are highly endothermic in the gas phase, the calculated $D_{e,g}$ values being CH_3–H, 4.85 eV; CH_2–H, 5.13 eV; CH–H, 4.93 eV; C–H, 3.72 eV. On the metal surfaces, there is significant reduction in the D_e values, owing to the presence of strong M–CH_{x-1} and M–H bonds. On Ru, the first and second dehydrogenation steps $CH_{x,s} \rightarrow CH_{x-1,s} + H_s$ ($x = 4, 3$) are nearly thermoneutral; the third and fourth steps ($x = 2, 1$) are slightly exothermic and endothermic, respectively. The estimated activation barriers are 0.6–1.2 eV. On Os, one step is slightly exothermic, two steps are slightly endothermic, and one step is mildly endothermic. The corresponding barriers are 0.8–1.3 eV. On Rh, there are one mildly exothermic step, one slightly exothermic step, and two slightly endothermic steps. On the coinage metals, all steps are rather endothermic. The large dissociation energies correspond to higher activation barriers. For the whole process, the reaction with the highest activation barrier should be the rate-determining step (RDS). Among the transition metals, however, the highest barriers are rather similar. So from these results, it is not easy to predict the trend in the catalytic activities within the transition metals. We consider another quantity.

Summation of the energies for the four discrete steps gives the total dissociation energies $D_{e,s}^{tot}$ for $CH_{4,s} \rightarrow C_s + 4H_s$. It should be a more realistic measure for the activity of the metal in methane dissociation. A comparison of the $D_{e,s}^{tot}$ values is given in Table 4 and schematically shown in Fig. 3. The total dissociation is shown to be quite exothermic on Rh (by −0.7 eV); it is slightly endothermic on Ru (0.01 eV) and Ir (0.3 eV), and it is rather endothermic on Os, Pd, and Pt (∼1 eV). This indicates that the total dissociation of methane on Rh is thermodynamically the most favorable among the transition metals being considered. The

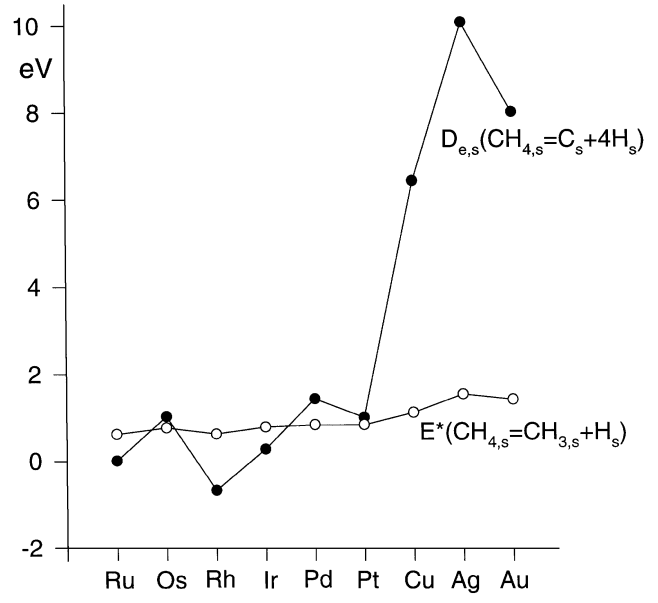

FIG. 3. Schematic illustration of calculated total dissociation energies $D_{e,s}$ for the complete dissociation of methane ($CH_{4,s} \rightarrow C_s + 4H_s$) and activation energies E^* for the abstraction of the first hydrogen atom from methane ($CH_{4,s} \rightarrow CH_{3,s} + H_s$).

$D_{e,s}^{tot}$ values vary in the order Rh < Ru < Ir < Os ≈ Pt < Pd. In the OMS experiments of Schmidt *et al.* (6), the methane conversions were found to be 80% on Rh, 73% on Ir, 67% on Pt, and 56% on Pd. The trend in the total dissociation energies is in line with the experimentally observed tendency over the metals. On the coinage metals, the total dissociation is shown to be very endothermic, with $D_{e,s}^{tot}$ values more than 5 eV (115 kcal/mol). There are two causes for the high endothermicities. On one hand, the adsorption energy of H on the coinage metal is relatively small as compared with those on the other transition metals. On the other hand, the adsorption energy of CH_x on the coinage metal increases only weakly from $x = 3$ to $x = 1$ and even decreases from $x = 1$ to $x = 0$. Therefore, a complete dissociation of CH_4 to surface C_s and H_s is difficult on the coinage metals, in agreement with the experimental fact that coinage metals are inactive in OMS reaction. The reaction endothermicity increases from Cu → Au → Ag.

Oxygen-Assisted Dissociation

According to Eq. [3], there are atomic oxygens on the metal surface. Therefore, in addition to the direct dissociation of methane on bare metal surface, we may consider the following reactions:

$$CH_{x,s} + O_s \rightarrow CH_{x-1,s} + OH_s \quad (x = 4, 3, 2, 1). \qquad [10]$$

The dissociation of methane on Rh in the presence of O_s was investigated by applying the BOC-MP model (14), where different surface oxygens at on-top, bridge, and hollow sites were examined. The BOC-MP results show that oxygen atom at on-top sites promotes methane dehydrogenation. Here we consider the adsorbed O_s at on-top and hollow sites only. The differences (Δ) between the dissociation energies with and without the involvement of chemisorbed oxygens are given in Table 6.

Because the H atom binds more strongly with O_s^{top} than with the bare metal, the methane dissociation reactions in the presence of O_s located at on-top sites have lower reaction energies due to hydroxyl formation. This means that O_s^{top} promotes the dehydrogenation of CH_x, in agreement with the BOC-MP predictions (14). However, the Δ^{top} values may be rather different for different metals. They are in fact very small for Ru, Os, and Rh, but large for Cu, Ag, and Au. The O species at the hollow site, O_s^{hol}, shows different behavior toward methane dissociation. O_s^{hol} increases the adsorption energies of H on Pt and coinage metals, but decreases those on the other transition metals. Therefore, on Pt and Cu–Au, O_s^{hol} also promotes methane dissociation, but not as strongly as O_s^{top}. On the other transition metals, the presence of O_s^{hol} does not promote methane dissociation. Because the Δ values for Cu–Au are very negative, significant methane dissociation on these metals would be likely if there is a larger amount of O_s species on the surface. There is experimental evidence that methane could react with supported CuO to produce CO_2 and H_2O (12).

H_2, CO, CO_2, and H_2O Formation

Equations [5] and [6] show that adsorbed H atoms combine to form H_2, and adsorbed C_s reacts with O_s to produce CO. On the other hand, byproducts (CO_2, H_2O) may be generated according to the reactions

$$CO_g + O_s \rightarrow CO_{2,s} \rightarrow CO_{2,g} \qquad [11]$$

$$H_s + OH_s \rightarrow H_2O_s \rightarrow H_2O_g. \qquad [12]$$

TABLE 6

Difference (Δ in eV) between the Dissociation Energies with and without the Involvement of Chemisorbed Oxygens

		Δ^{top} (O at on-top)	Δ^{hol} (O at hollow)
$CH_{x,s} + O_s \rightarrow CH_{x-1,s} + OH_s$	Ru_{10}	−0.06	+0.08
	Os_{10}	−0.03	+0.23
	Rh_{10}	−0.05	+0.32
	Ir_{10}	−0.46	+0.13
	Pd_{10}	−0.68	+0.13
	Pt_{10}	−0.75	−0.32
	Cu_{10}	−2.37	−0.55
	Ag_{10}	−3.12	−1.88
	Au_{10}	−2.87	−1.37

Note. s, surface.

TABLE 7

Calculated Combination (or Desorption) Energies (eV)

	Ru_{10}	Os_{10}	Rh_{10}	Ir_{10}	Pd_{10}	Pt_{10}	Cu_{10}	Ag_{10}	Au_{10}
$H_s + H_s \rightarrow H_{2,s}$	0.82	0.52	0.96	0.60	0.40	0.46	−0.58	−1.56	−1.20
$C_s + O_s \rightarrow CO_s$[a]	0.12	0.28	0.75	−0.13	−2.55	−1.91	−3.60	−6.17	−5.64
$CO_s \rightarrow CO_g$	1.64	1.05	1.84	1.53	1.46	1.70	0.55	0.19	0.30
Exptl[b]	1.26		1.43		1.47	1.43	0.63	0.26	
$CO_g + O_s \rightarrow CO_{2,s}$	−0.22	−0.31	0.21	−0.84	−2.37	−2.22	−1.39	−2.86	−3.34
$H_s + O_s \rightarrow OH_s$	0.08	0.23	0.93	0.13	0.10	−0.27	−0.55	−1.88	−1.37
$H_s + HO_s \rightarrow H_2O_s$	1.19	0.65	0.91	0.30	−1.40	−0.82	−0.75	−1.87	−2.50
$CH_{3,s} + CH_{3,s} \rightarrow C_2H_{6,g}$	−0.06	−0.36	−0.32	−0.54	−0.98	−0.52	−1.76	−3.12	−2.56
$CH_{2,s} + CH_{2,s} \rightarrow C_2H_{4,g}$	0.69	0.49	0.91	0.83	−0.93	−0.51	−1.81	−4.09	−3.53
$CH_s + CH_s \rightarrow C_2H_{2,g}$	2.96	3.02	3.62	3.76	0.82	2.76	−1.66	−4.62	−2.28

Note. g, gas; s, surface.

[a] On Ru, Rh, Ir, Pd, and Pt, CO prefers the hollow site, whereas on Os, Cu, Ag, and Au, CO prefers the on-top site.

[b] Experimental adsorption energies of CO, cited from Ref. (18).

It has been shown (Table 4) that the complete dissociation of CH_4 to surface C_s and H_s is difficult on the coinage metals. In Table 7 we have also listed the calculated combination energies on Cu–Au. The rather negative values indicate that all the combination reactions (for both syngas and byproducts formations) on Cu–Au are very favorable. This is in concord with the mentioned experimental fact that methane can react with supported CuO to produce CO_2 and H_2O.

On Ru–Pt, additional energy is required for the combination reaction of $H_s + H_s$; it is endothermic by 0.4–1 eV, depending on the metal. The formations of H_2 on Ru and Rh are somewhat more endothermic than on the other transition metals. Because H_2 is a very stable saturated molecule, the subsequent desorptions are easy (the calculated desorption energies of H_2 are nearly zero). The same is true for CO_2 and H_2O.

The combination energies of $C_s + O_s$ are rather different for different metals. On Pd and Pt, the combination reactions are very exothermic, thereby proceeding easily. On Rh, the combination is mildly endothermic. On the other three metals (Ru, Os, Ir), the combinations are nearly thermoneutral.

The desorptions of CO_s on the transition metals (Ru–Pt) are rather endothermic. This is because there exists a relatively strong binding between the metal surface and CO. The binding of CO to the coinage metals is weak. Experimental adsorption energies of CO are known for many metals. All the calculated values are in good agreement with the available experimental data.

The formations of CO_2 from $CO_g + O_s$ are energetically favorable, especially on Pd and Pt. So, adsorbed atomic O species still have a strong ability to oxidize CO_g to CO_2. Of course, compared with a free O, the oxidation ability of an adsorbed O is much less. So the formation of CO_2 in inevitable, in agreement with experimental observation. On the other hand, the CO_2 selectivity would be dependent on the amount of adsorbed oxygen present on the metal surface. This conclusion agrees with the experimental fact (5c, 14) that on an oxygen-rich surface, the selectivity of CO_2 was higher than that of CO and with the consumption of surface oxygen, CO selectivity rises while the CO_2 selectivity falls.

The $O_s + H_s \rightarrow OH_s$ reaction on Rh is shown to be significantly more endothermic than on the other transition metals. On Pt the reaction is even exothermic. Experimental observation (5c) showed that the OH formation by the reaction is more favorable on Pt than on Rh, which is consistent with the trend in the calculated values. Because the relative instability of OH on Rh would curtail the formation of H_2O, one expects higher H_2 selectivity on Rh than on Pt. This is also in accord with experimental finding (5c, 6). The calculated results show that the formation of H_2O from $OH_s + O_s$ is much less favorable on Rh than on Pt. This can also explain the difference in H_2 selectivity between Rh and Pt. The summation of the energies of $(H_s + O_s \rightarrow HO_s) + (H_s + HO_s \rightarrow H_2O)$ is a measure of the metal selectivity of H_2O, which follows the order of $Rh < Ru < Os < Ir < Pt < Pd$. In Fig. 4, we show plots of the combination energies for the four combination reactions versus the metals.

$CH_{x,s}$ Couplings

Table 1 shows that the adsorption energies of H on the metal surface are less than 3 eV, which is much smaller than the energy required to break the tetrahedral C–H bond in CH_4 (the calculated and experimental CH_3–H bond energies are 4.85 and 4.51 eV, respectively). Therefore the generation of a gas-phase CH_3 radical via H-abstraction from CH_4 on the metal surface is unlikely. However, one cannot rule out the possibility for the couplings of the surface

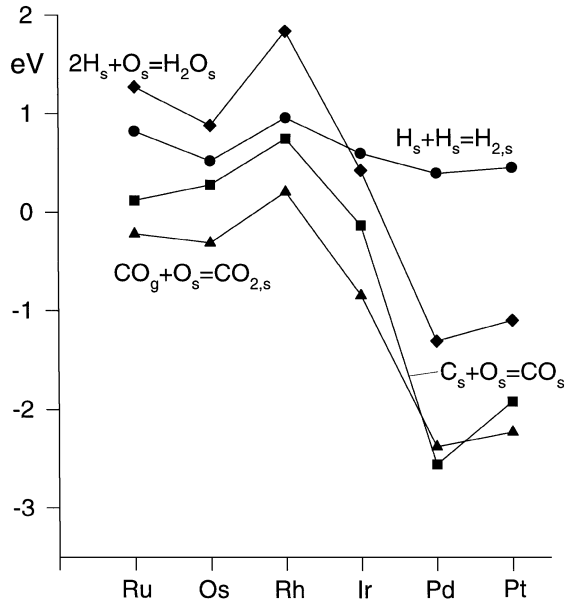

FIG. 4. Schematic illustration of calculated combination energies for syngas and byproduct formations.

species $CH_{x,s}$:

$$CH_{x,s} + CH_{x,s} \rightarrow C_2H_{2x,g} \quad (x = 3, 2, 1). \qquad [13]$$

In this section, we make an examination for the energetics of the $CH_{x,s}$ coupling processes. The calculated combination energies of Eq. [13] are given in Table 7 and schematically shown in Fig. 5.

A general tendency is that with decreasing x, there is decreasing mobility of CH_x to couple. The combination reactions of $CH_{3,s} + CH_{3,s} \rightarrow C_2H_6$ are exothermic on all the transition metals. This means that the coupling of $CH_{3,s}$ will compete with the dissociation process. Among the transition metals, the reaction on Pd is the most exothermic. The combination $2CH_{2,s} \rightarrow C_2H_4$ is endothermic (by 0.5–0.9 eV) on Ru–Ir, but exothermic on Pd and Pt, where the reaction on Pd is more exothermic than on Pt. The combination $2CH_s \rightarrow C_2H_2$ is highly endothermic on Ru–Ir and Pt, but only mildly endothermic on Pd. These results suggest that the coupling reactions on Pd are energetically the most favorable, and Pt shows higher ability than the rest of the transition metals to mediate C_2 formation. In the OMS experiments of Tornianen and Schmidt (6), C_2 production was up to 14% selectivity over Pd, 2.4–4.0% over Pt, and less than 0.1% over other metals. The trend in the calculated combination energies is in full agreement with the experimental observations. Because the binding of CH_x to the coinage metal is relatively weak, all the coupling reactions on Cu–Au are shown to be strongly exothermic.

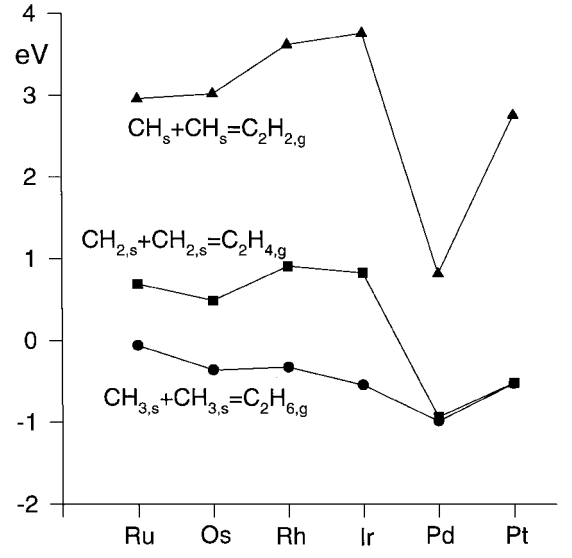

FIG. 5. Schematic illustration of calculated combination energies for $CH_{x,s} + CH_{x,s} \rightarrow C_2H_{2x,g}$.

CONCLUSIONS

The calculated results (for both dissociation and combination energies) provide a theoretical picture for the understanding of methane dissociation and syngas formation on the various transition metals. (i) The difference in methane conversions for the metals can be understood by the comparison of the total dissociation energies D^{tot} on the metals. According to the trend in the calculated D^{tot}, the most efficient catalyst for methane dissociation is Rh, which therefore gives a high CH_4 conversion; Ru and Ir are more active than Os, Pd, and Pt; the Cu, Ag, and Au metal catalysts do not mediate methane dissociation. (ii) The presence of oxygen located at metal on-top sites increases the adsorption energy of H, thereby promoting methane dehydrogenation; oxygen at hollow sites promotes methane dehydrogenation on Pt, Cu, Ag, and Au, but exerts an opposite effect to that on Ru–Pd. (iii) Although O species bind strongly to the metal surfaces, they possess the ability to oxidize CO_g to CO_2. Therefore on an oxygen-rich surface, the selectivity of CO_2 would be high. The formations of CO_2 occur more easily on Ir, Pd, and Pt than on Ru, Os, and Rh. (iv) On Pd and Pt, $2H_s + O_s$ can proceed easily to form H_2O. Therefore, Pd and Pt gave relatively low H_2 selectivities. (v) The $CH_{x,s}$ coupling reactions on Pd are much more favorable than on the other transition metals. Therefore, Pd yielded much higher C_2 production.

ACKNOWLEDGMENT

This work was supported by a Faculty Research Grant (FRG/96-97/II-99) of the Hong Kong Baptist University and by the Natural Science Foundation of Fujian Province, P. R. China.

REFERENCES

1. Krylov, O. V., *Catal. Today* **18**, 209 (1993).
2. (a) Vernon, P. D. F., Green, M. L. H., Cheetham, A. K., and Ashcroft, A. T., *Catal. Lett.* **6**, 181 (1990); (b) Vernon, P. D. F., Green, M. L. H., Cheetham, A. K., and Ashcorft, A. T., *Catal. Today* **13**, 417 (1992).
3. Dissanayyake, D., Rosynek, M. P., Kharas, K. C. C., and Lunsford, J. H., *J. Catal.* **132**, 117 (1191).
4. (a) Boucouvalas, Y., Zhang, Z. L., and Verykios, X. E., *Catal. Lett.* **27**, 131 (1994); (b) Zhang, Z. L., and Verykios, X. E., *J. Chem. Soc. Chem. Commun.*, 71 (1995).
5. (a) Hickman, D. A., and Schmidt, L. D., *J. Catal.* **138**, 267 (1992); (b) Hickman, D. A., and Schmidt, L. D., *Science* **259**, 343 (1993); (c) Hickman, D. A., Haupfear, E. A., and Schmidt, L. D., *Catal. Lett.* **17**, 223 (1993).
6. (a) Torniainen, P. M., Chu, X., and Schmidt, L. D., *J. Catal.* **146**, 1 (1994); (b) Bharadwaj, S. S., and Schmidt, L. D., *J. Catal.* **146**, 11 (1994).
7. Choudhary, V. R., Rane, V. H., and Rajput, A. M., *Catal. Lett.* **22**, 289 (1993).
8. (a) Erdöhelyi, A., Cserényi, J., and Solymosi, F., *J. Catal.* **141**, 287 (1993); (b) Solymosi, F., Erdöhelyi, A., and Cserényi, J., *Catal. Lett.* **16**, 399 (1992).
9. Mallens, E. P. J., Hoebink, J. H. B. J., and Marin, G. B., *Catal. Lett.* **33**, 291 (1995).
10. (a) Buyevskaya, O. V., Wolf, D., and Baerns, M., *Catal. Lett.* **29**, 249 (1994); (b) Walter, K., Buyevskaya, O. V., Wolf, D., and Baerns, M., *Catal. Lett.* **29**, 261 (1994).
11. (a) Au, C. T., Hu, Y. H., and Wan, H. L., *Catal. Lett.* **27**, 199 (1994); (b) Au, C. T., Hu, Y. H., and Wan, H. L., *Catal. Lett.* **36**, 159 (1996); (c) Wang, H. Y., and Au, C. T., *Catal. Lett.* **38**, 77 (1996).
12. Au, C. T., Wang, H. Y., and Wan, H. L., *J. Catal.* **158**, 343 (1996).
13. (a) Hu, Y. H., and Ruckenstein, E., *J. Catal.* **158**, 260 (1996); (b) Hu, Y. H., and Ruckenstein, E., *Catal. Lett.* **34**, 41 (1995); (c) Ruckenstein, E., and Hu, Y. H., *Catal. Lett.* **35**, 265 (1995).
14. Au, C. T., and Wang, H. Y., *J. Catal.* **167**, 337 (1997).
15. Prettre, M., Eichner, C., and Perrin, M., *J. Chem. Soc. Faraday Trans.* **43**, 335 (1946).
16. Au, C.-T., Liao, M.-S., and Ng, C.-F., *J. Phys. Chem.* **102**, 3959 (1998).
17. Shustorovich, E., and Baetzold, R. C., *Science* **227**, 876 (1985).
18. Shustorovich, E., *Adv. Catal.* **37**, 101 (1990).
19. Shustorovich, E., and Sellers, H., *Surf. Sci. Rep.* **31**, 1 (1998).
20. ADF program package, version 2.0.1: (a) Baerends, E. J., Ellis, D. E., and Ros, P., *Chem. Phys.* **2**, 41 (1973); (b) te Velde, G., and Baerends, E. J., *J. Comp. Phys.* **99**, 84 (1992).
21. Ziegler, T., and Rauk, A., *Theoret. Chim. Acta* **46**, 1 (1977).
22. Ziegler, T., Tschinke, V., Baerends, E. J., Snijders, J. G., and Ravenek, W., *J. Phys. Chem.* **93**, 3050 (1989).
23. Vosko, S. H., Wilk, L., and Nusair, M., *Can. J. Phys.* **58**, 1200 (1980).
24. Becke, A. D., *Phys. Rev.* **A38**, 3098 (1988).
25. Perdew, J. P., and Wang, Y., *Phys. Rev.* **B33**, 8800 (1986).
26. Stoll, H., Pavlidou, C. M. E., and Preuss, H., *Theoret. Chim. Acta* **49**, 143 (1978).
27. Perdew, J. P., *Phys. Rev.* **B33**, 8822 (1986).
28. Hermann, K., Bagus, P. S., and Nelin, C. J., *Phys. Rev.* **B35**, 9467 (1987).
29. Panas, I., Schüle, J., Siegbahn, P., and Wahlgren, U., *Chem. Phys. Lett.* **149**, 256 (1988).
30. Zheng, C., Apeloig, Y., and Hoffmann, R., *J. Am. Chem. Soc.* **110**, 749 (1988).
31. Torras, J., Ricart, J. M., Illas, F., and Rubio, J., *Surf. Sci.* **297**, 57 (1993).
32. Illas, F., Zurita, S., Rubio, J., and Márquez, A. M., *Phys. Rev.* **B52**, 12372 (1995).
33. Bauschlicher, C. W., Jr., and Bagus, P. S., *J. Chem. Phys.* **81**, 5889 (1984).
34. Chang, H., Harrison, J. F., Kaplan, T. A., and Mahanti, S. D., *Phys. Rev.* **B49**, 15753 (1994).
35. Reed, A. E., Weinstock, R. B., and Weinhold, F., *J. Chem. Phys.* **83**, 735 (1985).
36. Anton, A. B., and Cadogan, D. C., *Surf. Sci.* **239**, L548 (1990).
37. Campbell, R. A., Szanyi, J., Lenz, P., and Goodman, D. W., *Catal. Lett.* **17**, 39 (1993).
38. Kratzer, P., Hammer, B., and Nørskov, J. K., *J. Chem. Phys.* **105**, 5595 (1996).
39. Stewart, C. N., and Ehrlich, G., *J. Chem. Phys.* **62**, 4672 (1975).
40. Brass, S. G., and Ehrlich, G., *Surf. Sci.* **187**, 21 (1987).
41. Luntz, A. C., and Harris, J., *Surf. Sci.* **258**, 397 (1991).
42. Schoofs, G. R., Arumainayagam, C. R., McMaster, M. C., and Madix, R. J., *Surf. Sci.* **215**, 1 (1989).
43. Hamza, A. V., Steinrück, H.-P., and Madix, R. J., *J. Chem. Phys.* **86**, 6506 (1987).
44. Anderson, A. B., and Maloney, J. J., *J. Phys. Chem.* **92**, 809 (1988).
45. Blomberg, M. R. A., Siegbahn, P. E. M., Nagashima, U., and Wennerberg, J., *J. Am. Chem. Soc.* **113**, 424 (1991).
46. Swang, O., Faegri, K., Jr., and Gropen, O., *J. Phys. Chem.* **98**, 3006 (1994).